Journal of Marine Research, 58, 465–491, 2000

Properties of vertical current shear across stratification in the North Sea

by Hans van Haren[1]

ABSTRACT

Observations from the central North Sea show that, as soon as thermal stratification becomes established by solar insolation in the spring, the vertical smoothly varying horizontal current structure observed in winter becomes distorted, with strongest vertical shear coincident with the strongest buoyancy gradients (thermoclines). This shear is predominant at the local *inertial* frequency following strong wind-forcing or when the thermocline thickness is relatively large, and the semidiurnal *tidal* frequency otherwise. Although the *currents* at these frequencies have a completely different character, being circularly polarized and mode-1 at the inertial frequency and almost rectilinear and barotropic at the tidal frequency, their *shear* vectors are both anticyclonically polarized. While this is understood for near-inertial motions, it is less obvious for vertically varying tidal currents, in the absence of internal tides.

Viscous flows are distinguished from those governed by inviscid physics by inspection of their vertical current structures. It is demonstrated that the tidal frictional bottom boundary layer not only determines the depth and 'thickness' of the thermocline in shelf seas, but also the fate of shear across the stratification. This shear is dominated by the change in phase of the anticyclonic rotary current component. The circular polarization of the shear vector implies that the shear magnitude varies much slower with time than its components, providing justification for the use of slowly varying exchange parameters in models. As stratification also varies with time much slower than the inertial period, a 'constant' eddy diffusivity is rendered through a marginal stability equilibrium relating shear and stratification and turbulent diapycnal exchange, irrespective of the generating frequency.

1. Introduction

Shelf seas are relatively shallow and have strong currents, usually dominated by tidal motions. Turbulent frictional processes are important in a substantial part of the water column (Soulsby, 1983, 1990), determining the fate of vertical buoyancy gradients (specified by a buoyancy frequency N) through associated mixing. When this mixing, imposed by stress at the external surface and bottom boundaries, is insufficient to homogenize the potential energy input by solar insolation or freshwater discharge, stratification (thermocline, for temperature stratification) increases away from the well-mixed boundary layers.

1. Netherlands Institute for Sea Research (NIOZ), P.O. Box 59, 1790 AB Den Burg, The Netherlands. ***email: hansvh@nioz.nl***

Increasing stratification *reduces* vertical turbulent exchange of momentum and mass, so that enhanced vertical current differences (*shear* $\mathbf{S} = [\partial u/\partial z, \partial v/\partial z]$, for horizontal east ($u$) and north ($v$) current components) are expected across such stratification. However, increasing shear may *enhance* vertical mixing internally (Munk and Anderson, 1948), possibly preceded by sharpening of the thermocline through the interaction of shear and horizontal density gradients ('stirring'; Eckart, 1948). Laboratory experiments (e.g. Linden, 1979 and references therein) show subtle interactions between shear and stratification and quite a range of different results in varying thicknesses of shear and stratification layering. As the flow becomes more stable, a current interface tends to become thicker than the density interface.

Observations from the central North Sea (Fig. 1) show that mid-depth shear, while larger than that in the frictional bottom boundary layer, is clearly concentrated at the stratification maximum, which may indicate active mixing is important (Linden, 1979). Components of this shear are enhanced at tidal or inertial frequencies (cf. Section 4). This paper analyzes primarily, in detail, properties of the observed enhanced shear across stratification and secondarily, implications of this shear for stability within the water column and mixing across the stratification.

The shear magnitude increases as soon as stratification is present, reaching a maximum in mid-summer, and showing short-term variations with time superposed on modulations varying slower than a day (Fig. 2). This dominant base of shear magnitude varying slowly with time is related to the (bottom) current magnitude inferred from the spring-neap cycle and wind-stress. Due to these properties, and the oscillatory nature of the shear components, the main analysis will be in terms of oscillatory Ekman dynamics, which have proven a useful description of average vertical structure of tidal currents in shelf seas (Maas and van Haren, 1987; Howarth, 1998). Enhanced shear across stratification also may be caused by mode-1 internal waves governed by inviscid physics. In the North Sea, dominant mode-1 structures have only been observed for inertial currents, with a modification by viscosity (Maas and van Haren, 1987), and for tidal currents near the Dutch coast (Visser *et al.,* 1994), but not for freely propagating internal tidal waves. After analyses of different arrays of current meters and thermistor strings moored in the central North Sea, van Haren and Maas (1987) and Howarth (1998) could find no evidence for internal tides.

In this paper, properties of shear across stratification are used to distinguish between currents governed by inviscid physics and Ekman dynamics. Consequently, the theory of Ekman dynamics outlined briefly in Section 2 is for barotropic oscillatory currents. It includes a neglected property of enhanced shear across stratification governed by viscosity. The more straightforward properties of inviscid mode-1 shear will be given throughout the paper, where appropriate. In Section 4, the general applicability of this aspect of Ekman dynamics will be tested for a single mooring site from the Integrated North Sea Programme (INP). The presentation of the data in Section 4 focuses on changes within relatively short time scales of less than a day to a week, under varying conditions, in contrast with the more general presentation of the vertical structure of currents averaged over 2–4 weeks by Maas and van Haren (1987). Further aspects related to Ekman shear will be discussed in Section

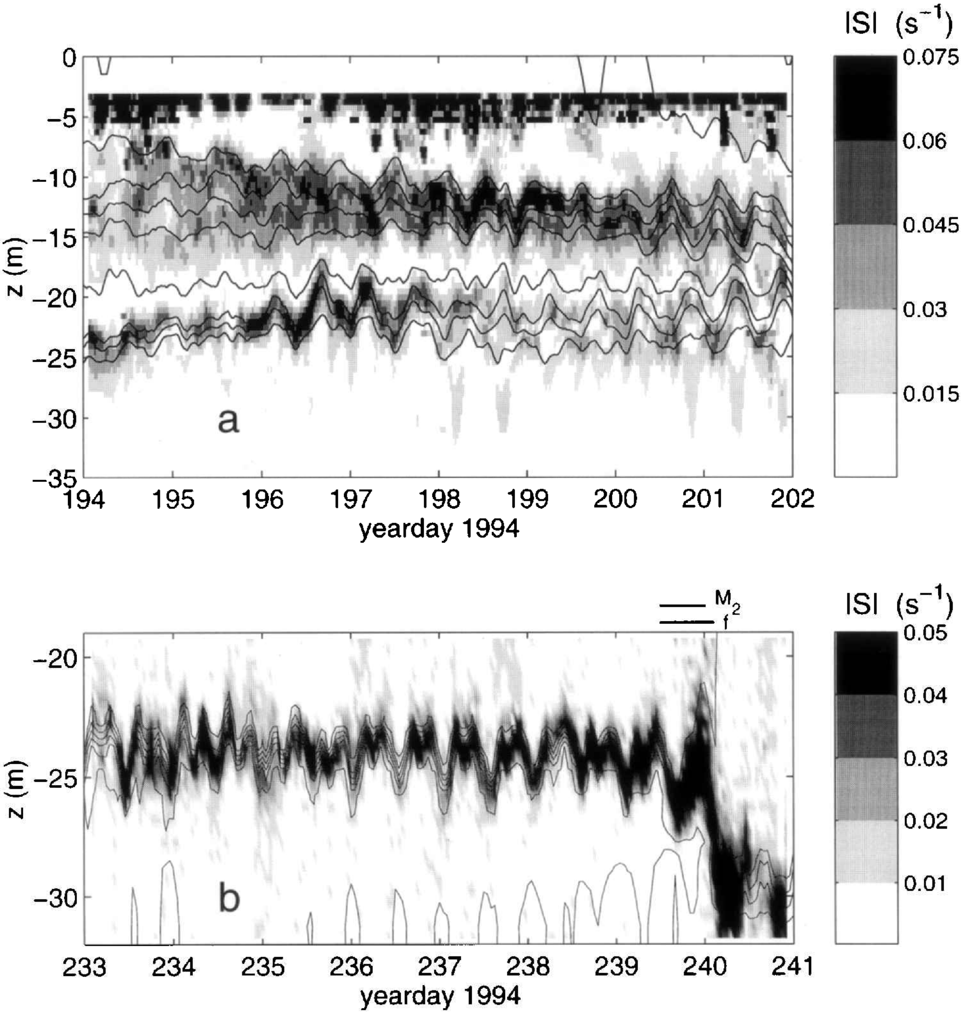

Figure 1. Sample time series of vertical current shear magnitude and stratification from ADCP and thermistor strings, respectively. Stratification is presented by solid isotherms drawn every 1°C, between 10–17°C. Shear has been computed at the 0.5 m vertical resolution of the ADCP measurements and smoothed over 1 m in depth and 1 hour in time prior to clipping the upper levels for displaying purposes. Bars between the graphs indicate tidal and inertial periods. Time is given according to the convention that January 1, 12.00 UTC equals yearday 0.5 (in 1994). (a) Mid-summer period. There are two major thermoclines and corresponding shear. (Observations contaminated by side-lobe interference above 5–8 m depth are black). (b) Late-summer period.

5, including a discussion on the differences between inertial and noninertial shear. Implications of the dominant shear components for vertical exchange of mass across stratification will be discussed in Section 6. As a measure for (in)stability for mixing, a gradient Richardson number ($Ri = N^2/|\mathbf{S}|^2$) will be computed from observations.

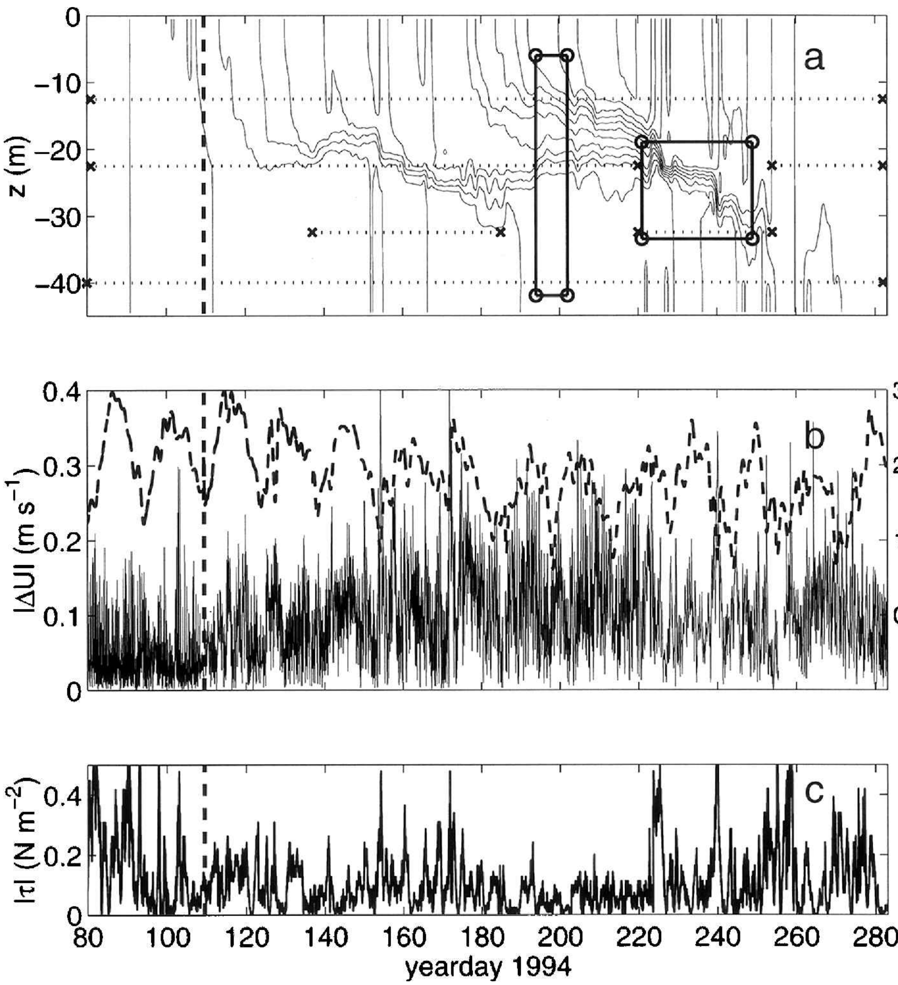

Figure 2. (a) Seasonal stratification from daily-filtered isotherms (thin solid lines, drawn every 1°C between 6–20°C) and a schematic of the time-depth distribution of current measurements. The solid (-○-) boxes indicate the (t, z) ranges of ADCP measurements. The dotted lines (. .**x**) indicate the (t, z) position and range of current meters. The heavy vertical dashed line indicates the onset of seasonal stratification. (b) Time-series of velocity differences $|\Delta U| = |(\Delta u, \Delta v)|$ across the stratification (thin solid line) and near-bottom current magnitude (dashed line, scale to the right). (c) Wind-stress magnitude $|\tau| = \rho_a C_d W^2$, where W denotes the wind speed measured at a platform 150 km to the southwest of the mooring, $C_d = 0.0015$ the constant drag coefficient and ρ_a the density of air.

2. Theory

Assuming horizontal oscillatory currents $[u, v](t, z)$ are represented by $u = Re[\tilde{u} \exp(-i\sigma' t)]$, with harmonic $\tilde{u} = U \exp(i\varphi_u)$ and similarly for v, oscillatory Ekman dynamics are most elegantly posed in terms of circular counter-rotating rotary current components (Gonella, 1972). As the four current ellipse parameters

$$\begin{aligned} U &= W_+ + W_- && \text{major-axis amplitude} \\ e &= (W_+ - W_-)/(W_+ + W_-) && \text{eccentricity} \\ \psi &= (\theta_- + \theta_+)/2 && \text{inclination} \\ \varphi &= (\theta_- - \theta_+)/2 && \text{phase} \end{aligned} \tag{1}$$

can be expressed in terms of radii $W_\pm$ and phases $\theta_\pm$ of two counter-rotating *circular* current components (Prandle, 1982), the current components are used to form the complex velocity (Maas and van Haren, 1987),

$$w = u + iv = w_+^* \exp(i\sigma' t) + w_- \exp(-i\sigma' t), \tag{2a}$$

where $(\ )^*$ denotes a complex conjugate, $i^2 = -1$, $\sigma' = \sigma/f$, σ the harmonic frequency, f the inertial frequency of the rotating frame of reference. Amplitudes

$$w_+ = \frac{\tilde{u} - i\tilde{v}}{2} = W_+ \exp(-i\theta_+) \qquad \text{the cyclonic rotary component} \tag{2b}$$

$$w_- = \frac{\tilde{u} + i\tilde{v}}{2} = W_- \exp(i\theta_-) \qquad \text{the anticyclonic rotary component.} \tag{2c}$$

The current ellipse adopts the rotation sense of the rotary component having the largest amplitude. In terms of the rotary components (2b, c) the nondimensional linear equations for oscillatory motions driven by a sea level gradient in the presence of turbulent friction read (scaling the velocity components with a typical velocity magnitude, time with $1/f$, z with the water depth and the horizontal coordinates with the Rossby radius of deformation),

$$\mp(1 \pm \sigma')w_\pm + \frac{1}{2}\nabla_\mp \zeta = \frac{\partial}{\partial z}\left(\frac{E}{2}\frac{\partial w_\pm}{\partial z}\right), \tag{3}$$

where

$$\nabla_\mp = \frac{\partial}{\partial x} \mp i\frac{\partial}{\partial y}, \qquad \zeta \text{ the harmonic sea level,}$$

and boundary conditions

$$\begin{aligned} \frac{\partial w_\pm}{\partial z} &= s w_\pm \quad && \text{at} \quad z = 0, \quad && \text{the bottom, and} \\ \frac{\partial w_\pm}{\partial z} &= 0 && \text{at} \quad z = 1, && \text{the surface.} \end{aligned} \tag{4}$$

Solutions to Eqs. (3) with boundary conditions (4) depend on two parameters, the internal stress parameter or Ekman number $E = 2A/fH^2$, where H is the water depth and A the turbulent eddy viscosity, and the ratio of bottom to internal stresses ('stress parameter') $s = rH/A$, with $r = 8/3\pi \times C_d U_b$, a bottom friction velocity related to the bottom drag coefficient C_d and U_b the oscillatory current amplitude at a reference level, typically 1 m above the bottom.

E varying with depth complicates the solutions. Using simple parametrizations for $E(z)$, Maas and van Haren (1987) successfully fitted the model (3–4) to their tidal current observations under well mixed (constant E) and stratified (piecewise constant E) conditions in the same North Sea area. This model will be used in Section 5 to demonstrate changes in vertical variations of amplitude and phase of the rotary current components upon variations in Ekman number. In theory, as will be shown here, Ekman dynamics exhibit a feature of barotropic current shear, which has been neglected so far.

Independent of the complexity of $E(z)$ (see Soulsby, 1990 for an overview), all solutions to (3–4) contain scaling heights or Ekman depths $\delta_\pm$ (Soulsby, 1983) over which the current profiles vary in the vertical. They are different for the two rotary components according to,

$$\delta_\pm = \gamma\sqrt{C/(|f \pm \sigma|)}, \qquad \gamma \text{ arbitrary and } C \text{ a typical friction parameter.} \tag{5}$$

The anticyclonic height of frictionally-modified currents is larger than the cyclonic, their ratio depending only on the frequency σ relative to the local inertial frequency with the largest deviations from a ratio of unity for frequencies closest to f.

The ratio of the two Ekman depths is $\delta_-/\delta_+ \approx 3$ for a semidiurnal tidal current at mid-latitudes. The frictional bottom boundary layer (δ) is determined by the weighted average $\delta = (|\hat{W}_+|\delta_+ + |\hat{W}_-|\delta_-)/|\hat{W}|$, where $|\hat{W}| = |\hat{W}_+| + |\hat{W}_-|$ and the hat denotes the vertical average (Soulsby, 1983). In the case of a nearly rectilinear oscillatory current, the anticyclonic rotary component δ_- dominates.

Assuming $|\hat{W}_+|\delta_+ < |\hat{W}_-|\delta_-$, the shear, expressed in terms of the rotary components (2b, c) at depths $2|\hat{W}_+|/|\hat{W}|\delta_+ \ll z < 2|\hat{W}_-|/|\hat{W}|\ \delta_-$, is

$$\begin{aligned} \frac{\partial w_+}{\partial z} &= \frac{1}{2}\left(\frac{\partial \tilde{u}}{\partial z} - i\frac{\partial \tilde{v}}{\partial z}\right) \approx 0 \\ \frac{\partial w_-}{\partial z} &= \frac{1}{2}\left(\frac{\partial \tilde{u}}{\partial z} + i\frac{\partial \tilde{v}}{\partial z}\right) \neq 0. \end{aligned} \tag{6}$$

That is, at depths sufficiently far above δ_+, but still within the range of the dominating anticyclonic Ekman depth, the vertical current shear of oscillatory motions can be expressed as a single rotary component,

$$\frac{\partial w}{\partial z} \approx \frac{\partial w_-}{\partial z} e^{-i\sigma' t} = \left(\frac{\partial W_-}{\partial z} + iW_-\ \frac{\partial \theta_-}{\partial z}\right) e^{i(\theta_- - \sigma' t)}. \tag{7}$$

Comparing (2c) and (7) reveals that the shear of a purely anticyclonic in time current, vertically varying in amplitude or phase, is also anticyclonically polarized in time. Thus, the shear *magnitude* is constant with time. Following (7), this holds for *any* oscillatory current in a rotating frame of reference irrespective of the degree of degeneracy of the current ellipse. In practice, it may particularly hold for $\sigma \approx f$, when the ratio of Ekman depths is largest. Furthermore, as the largest constituent of W_- governs the vertical extent of turbulent mixing in the (bottom) boundary layer, it determines the depth where the vertical density stratification imposed (by heating) from above becomes concentrated (for $\delta_- \leq H$). Once the water column is stratified, W_- determines the shear enhancement of its own major constituent due to local reduction of E by increased stratification, as will be shown in Section 5.

3. Data

The INP mooring is located in the central North Sea, Oyster Grounds, at 54°25′N, 04°02′E ($f = 1.118 \times 10^{-4}$ s^{-1}, $T_f \approx 14.7$ hours), in water depth $H = 45$ m. The bottom is relatively flat; major topographic features are at least 50 km away. In winter, horizontal currents are dominated by the semidiurnal tide (M_2, S_2, henceforth denoted by the dominating former) with the ellipse nearly rectilinear, the major axis directed zonally (so that $u \gg v$) and amplitudes varying between 20–30 cm s^{-1} (neap-spring). The tidal frictional boundary-layer depths δ_+, δ_- are typically 10 and 30 m, respectively (Maas and van Haren, 1987).

Between November 1993 and February 1995, moorings were deployed with different arrays of standard Aanderaa thermistor strings spanning the entire water column, with thermistors at least every 2 m, and NBA and Aanderaa current meters at nominal depths of 13, 23 or 33 and 40 m (Fig. 2a). During two short periods in mid- and late-summer, data were obtained using RDI-broadband acoustic Doppler current profilers (ADCP's) sampling at nominal 0.5 m vertical increments. Meteorological data were sampled continuously 100–300 km from the mooring.

All data have a common half-hourly time interval, but most instruments sampled faster (down to once per minute). As will be shown, shear across stratification varies on timescales of an hour or more, and is generated by motions that vary over horizontal length scales much larger than the beam spread of the ADCP. Unless otherwise indicated, the data presented in Section 4 have *not* been smoothed by harmonic analysis or digital filtering to show the relative importance of specific oscillatory motions and rapid changes in their properties under (sudden) varying conditions.

Preferably, the local gradient Richardson number near a thermocline is computed from thermistor string and ADCP data, so that the minimum vertical length scale is dictated by the distance between thermistors. When ADCP data are not available, vertical current differences from current meters straddling a major thermocline are understood as shear. The separation distance between the current meters is irrelevant. Most shear is in the thermocline (Fig. 1). *Ri* is computed using the thermocline thickness as the appropriate vertical lengthscale.

4. Observations of shear and stratification

In 1994, mid-depth stratification was well established between days 110–255, mainly by temperature (Fig. 2a). Stratification slowly increases during spring. By mid-summer, the surface-bottom temperature difference was 11°C, concentrated in two, 5 m thick thermoclines between the surface and mid-depth. After the first late-summer strong wind-forcing on day 223, stratification becomes concentrated in a single thermocline near mid-depth. It remains there until final breakdown. Detailed ADCP and thermistor string observations (Fig. 1) show mid-depth shear (up to 0.15 s^{-1}) concentrated in thin layers of enhanced stratification.

a. Well-established stratification

Following a moderate (12 m s^{-1}) wind event on day 140, the atmosphere is relatively calm for about 8 days and the 19 m depth stratification constant with time. Initially, mid-depth shear is nonrotating and constant with time, and relatively weak. It suddenly ramps up with the onset of the spring tide (Fig. 3 and Fig. 2b). About 1–1.5 semidiurnal tidal periods after its onset, Cartesian shear components are dominantly semidiurnal *tidal* and have almost equal amplitudes which remain more or less constant in time. These shear components are 90° out of phase, with $\partial v/\partial z$ leading $\partial u/\partial z$. Thus, apart from some jitter, the shear vector traverses a circle anticyclonically, as predicted by (6). In time, the maximum in $\partial v/\partial z$ occurs approximately when the u-current reaches its maximum. The v-current tends to have a phase difference of about 180° across the thermocline (Fig. 3b).

The tidal shear magnitude varies somewhat on days 149–150 before subsiding on day 151 as abruptly as it arose (Fig. 4). Shear remains relatively low for about a day (152, during neaps, cf. Fig. 2b). Then, as the wind speed increases to 16 m s^{-1} on days 153–154, the shear ramps up as before, now dominantly *inertial,* within 1.5 inertial periods. The weaker tidal shear is apparent from the amplitude modulation. Inertial shear amplitudes (Fig. 4) are about 1.5 times larger than tidal shear (Fig. 3). Note the similarity between increasing shear during tidally (day 141 in Fig. 3) and inertially dominated periods (day 154 in Fig. 4). Both show an initial overshoot compared with the constant value later.

The inertial shear components are equal in amplitude, and show a 90° phase difference with the v-component leading in time. The v-current is again approximately 180° out-of-phase across the thermocline. One cannot use Ekman dynamics directly to explain this anticyclonic circular rotation of the inertial shear vector with time, because δ_- becomes infinite at $\sigma = f$ (Section 5). This behavior is consistent with inertial motions being anticyclonically polarized in time (Gill, 1982).

Given the above properties, there is no great difference between inertial and tidal shear other than inertial motions appearing after passage of atmospheric disturbances and

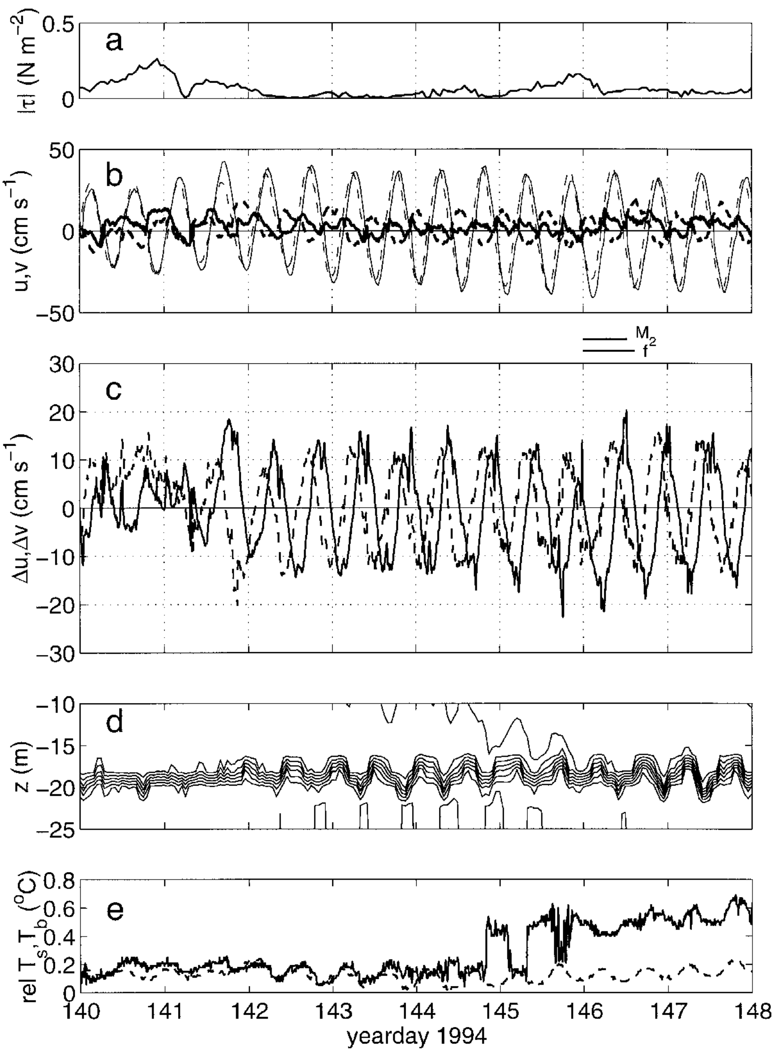

Figure 3. Example of *tidal* shear dominance across stratification in spring. (a) Wind-stress magnitude as in Figure 2c. (b) East (thin lines) and north (thick lines) *current* components measured at 12 m (solid lines) and 23 m depth (dashed lines). East currents dominate. (c) East (solid line) and north (dashed line) *current differences* between 12–23 m depth. (d) Isotherms drawn every 0.5°C, between 6.5–9.5°C based on 2 m temperature data. (e) Surface (T_s, solid line) and bottom (T_b, dashed line) temperatures offset to match at the start of depicted period.

semidiurnal tidal motions following the spring-neap cycle. However, their effects on the thermocline depth and stratification differ (compare Figs. 3d, e and 4d, e).

At the onset of tidal shear, the initially flat isotherms exhibit a tidal variation of 3 ± 1 m (Fig. 3d). This is not a manifestation of internal tides. These thermocline depth variations

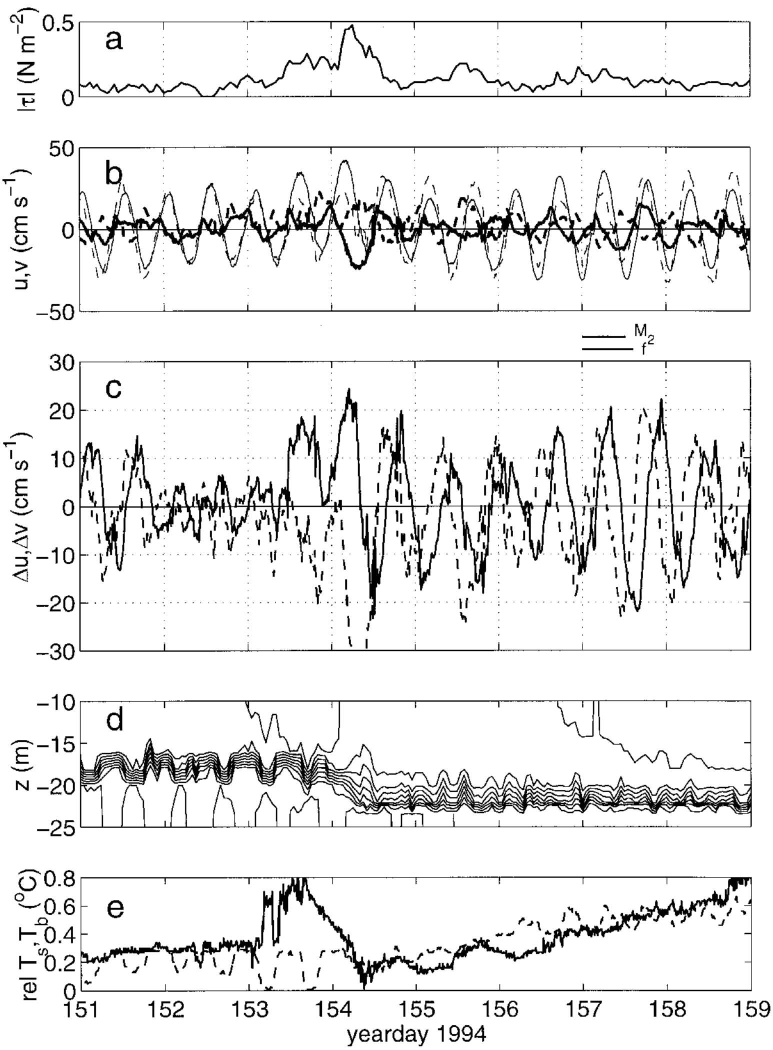

Figure 4. Example of *inertial* shear dominance across stratification in spring. (a) Wind-stress magnitude as in Figure 3a. (b) East (thin lines) and north (thick lines) *current* components measured at 12 m (solid lines) and 23 m depth (dashed lines). (c) East (solid line) and north (dashed line) *current differences* between 12–23 m depth. (d) Isotherms drawn every 0.5°C, between 7.0–11.0°C based on 2 m temperature data. (e) Surface (T_s, solid line) and bottom (T_b, dashed line) temperatures offset to match near the beginning of depicted period.

result from tidal and differential advection of an internal front, probably following local mixing events as shown by van Haren and Maas (1987) and Howarth (1998). Given the constant thermocline thickness of 2 m and an evenly spread shear therein, $Ri \approx 1$ most of the time, and decreases to 0.25 during short periods when the shear spikes to $\pm 0.1\ \mathrm{s}^{-1}$.

These high-shear, low-*Ri* events occur during periods near *u*-current reversal. They are partially attributable to stalling of the current meter vane, yielding an error of about 5 cm s^{-1}.[2] After correction $0.5 < Ri < 1$.

During the onset of inertial shear, the mean thermocline thickens by 3 m. Based on this thickening, and the associated in(de)crease of bottom (surface) temperatures (Fig. 4d, e), the inertial shear seems to cause vertical mixing. After this event on day 154, the thermocline shows weak vertical displacements and remains thicker, while the bottom temperature increases at about the same rate as the surface temperature due to atmospheric heating, evidence of continued vertical mixing at an average turbulent diffusivity of about $K = 5 \times 10^{-5}$ m^2 s^{-1}. Given an average thermocline thickness of 3–4 m, the average $Ri \approx 0.5$ for the period in Figure 4 (generally lower than for tidal shear alone), so that $|\partial u/\partial z| = |\partial v/\partial z| \approx N$.

The dominance of mid-depth semidiurnal tidal and inertial *shear* remains as long as the water column is stratified. During extended periods of calm weather in mid-summer, when the stratification extends close to the sea surface (Fig. 2), inertial shear dominates. Both inertially (mid-summer) or tidally dominated (late-summer) shear exhibit the same circularly polarized, anticyclonic rotary behavior (Fig. 5). The near-rectilinear *current* 'ellipses' are more erratic than shear, current paths often showing switchback behavior (Fig. 5c–d). This indicates a nonlinear cross-flow component of which the first tidal harmonic is the most important. This harmonic component dominates current spectra outside the semidiurnal tidal/inertial frequency band. Possible implications will be discussed further in Section 6. We continue with a description of the change in shear properties at the transition from well mixed to stratified conditions.

b. The onset of stratification

In winter, when the water column appears well mixed, mid-depth oscillating shear does not show circular time behavior (Fig. 6). Instead, it is erratic, the spectrum flat and featureless and not dominated at a single frequency. One exception is the fourth-daily appearance of spikes of up to about 1-hour duration around the onset of major current component reversal. These features were also observed during the well-stratified period.

However, as soon as even weak stratification is found anywhere in the water column lasting longer than a tidal cycle, the shear changes abruptly to semidiurnal tidal (or inertial) dominance, while the fourth-daily spikes decrease in magnitude. Although wind-stress is relatively weak during the presented stable stratified period between days 95–97 prior to the summer stratified period, the major thermocline ($\Delta T = 0.15$°C only) is mid-depth as

2. This value results from limited comparison between wintertime ADCP and simultaneously sampled current meter data indicating that the spikes occur more frequently and vigorously (but not exclusively) when current ellipses are nearly rectilinear, during high wind speeds (cf. Section 3b) and when sampled by mechanical devices. This is partially due to the imperfect response of current meters to surface wave action (e.g., Sherwin, 1988). However, spikes are also either due to the variations in the oscillatory vertical current structure as a function of phase in the cycle (Lamb, 1975), or to nonlinear (higher harmonic) current variations over extremely short horizontal scales, which are smoothed by an ADCP.

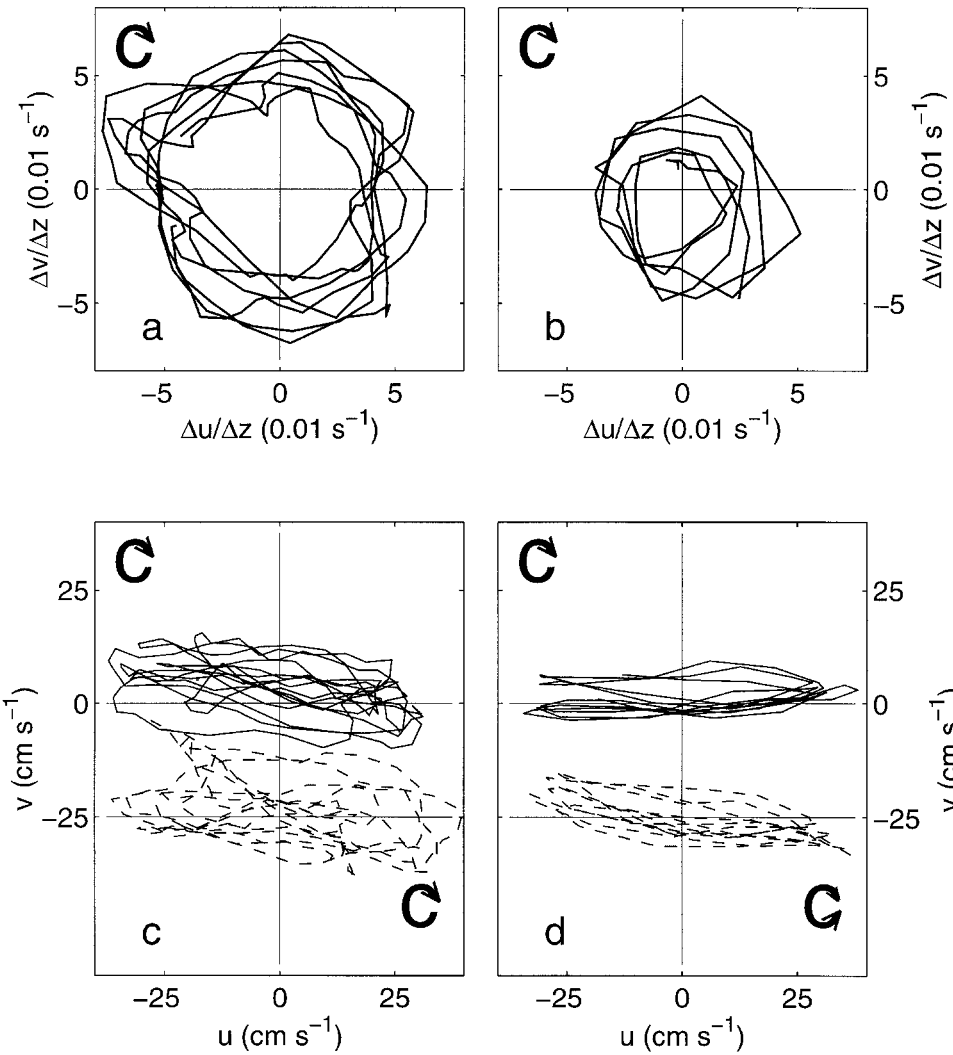

Figure 5. Observed ellipticity of mid-depth shear and current vectors from hourly subsampled data. The arrows indicate the sense of rotation. (a) From mid-summer days 196–200, predominantly *inertial shear* between 12 and 13 m depth. (b) From late-summer period days 234.7–237.2, predominantly *tidal shear* between 19 and 28 m depth, normalized by a constant 2 m thermocline thickness. (c) From the same period as (a), *current* ellipses at 11.5 (solid line) and 13.5 m depth (offset; dashed line). (d) From the same period as (b), *current* ellipses at 19 (solid line) and 28 m depth (offset; dashed line). The predominantly rectilinear current ellipses show a switchback behavior, so that the sense of rotation changes sign over a (tidal, inertial) period. The dominant sense of rotation is indicated by the heavy arrowhead. In the right-hand corner, the lesser dominant sense is indicated.

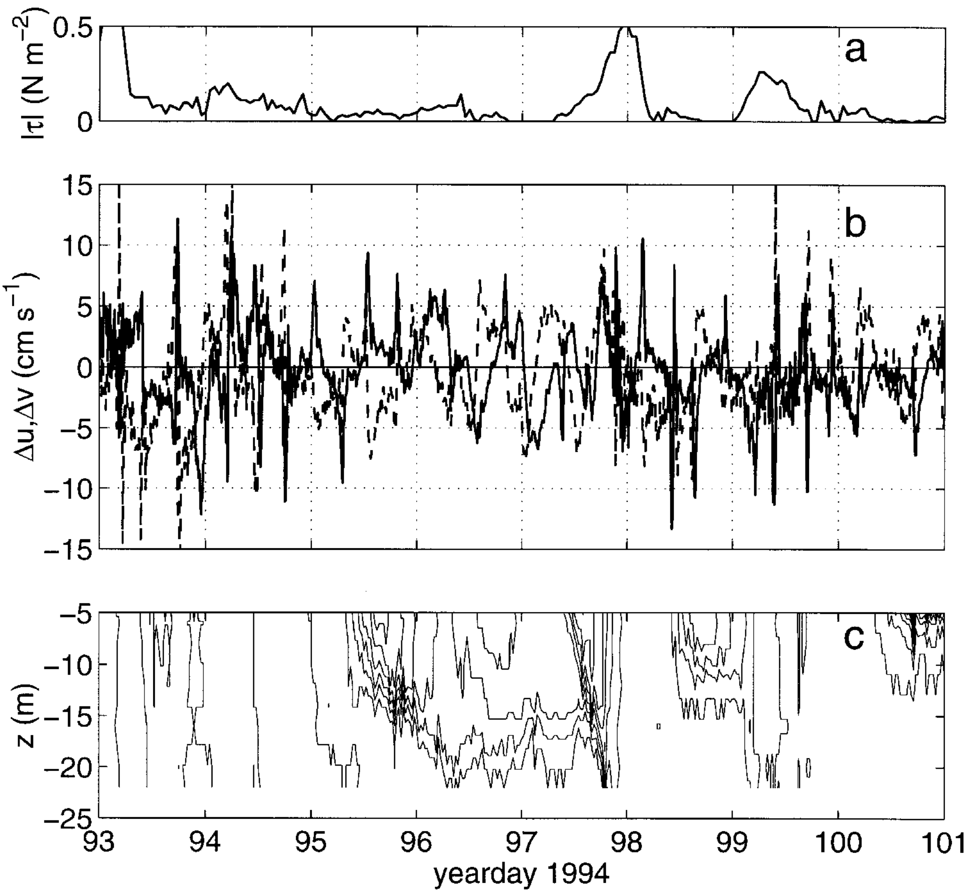

Figure 6. Example of shear across weak temporary stratification in early spring. (a) Wind-stress magnitude as in Figure 3a. (b) East (solid line) and north (dashed line) *current differences* across 12–23 m depth. (c) Isotherms every 0.05°C, between 5.8–6.4°C based on 2 m temperature data.

before, following nighttime convective cooling. After this mixing, from day 96.3 onward, anticyclonic rotation in time is established. It is destroyed a day later by enhanced wind mixing in concert with nighttime convection. These properties are not only manifest in spring, just before the onset of a stable seasonal stratification, but throughout winter.

From such observations, it may be tentatively concluded that the oscillatory vertical current profile rapidly responds to variations in vertical density structure within the water column. The response is such that mid-depth shear comes to equilibrium ($Ri \approx$ constant) with the enhanced stratification. This is partially caused by the shear being weighed in frequency, favoring near-inertial frequencies. The rotating water column acts as a band-pass filter so that only a monochromatic, circularly polarized (tidal or inertial) shear vector dominates. These observations will be compared with properties of Ekman dynamics.

5. Ekman dynamics properties of vertical current shear

We consider the Ekman dynamics model (3–4) for constant s and E, so that $C = 2A$ in (5), which matched vertical tidal current observations averaged over four weeks in the central North Sea under well-mixed conditions (Maas and van Haren, 1987). Model profiles show veering and phase advance of the current ellipse with depth (Fig. 7a, b). Observations are not reproduced in this figure, as the best-fitting profiles are all within one standard deviation of accuracy of current measurements.

Using their model to describe observations from a stratified water column, Maas and van Haren (1987) found best-fit constant vertical eddy viscosities $A_1 = A_3 \approx 2 \times 10^{-3}$ m^2 s^{-1} in surface (subscript 1) and bottom (3) boundary layers, as found during well mixed conditions, and a constant weakly turbulent $A_2 \approx 6 \times 10^{-5}$ m^2 s^{-1} $= 0.03\, A_1$ for a 10 m thick thermocline at mid-depth. No-slip bottom ($s \rightarrow \infty$) and stress-free surface boundary conditions are imposed, respectively. Continuity of velocity and stress are included across the internal boundaries between the different layers. Model profiles that match tidal currents averaged over two weeks show jumps of about 30° in θ_- and 10% in W_- (dashed lines in Fig. 7e, f).

These results are extended here, hypothesizing that Ekman dynamics with a time-invariant internal momentum transfer coefficient is adequate to describe the average tidal shear. Some properties of the observed time-dependent shear are studied qualitatively using the same model while varying $E_1(A_1)$ and $E_2(A_2)$, providing *a posteriori* justification for using (nearly) time-independent stress parameters.

A factor of 1.5 increase in tidal current amplitude, as observed from neap to spring, results in a factor-of-two increase in A_3 (and A_1), so that the Ekman depths increase by a factor of 1.5 as well. This may be sufficient for the dominant anticyclonic rotary component to be modified by the thermocline. While mid-depth anticyclonic shear does not vary dramatically under well-mixed conditions on such variation of $E(A)$ (Fig. 7c, d), especially the phase change with depth is augmented when stratification affects the vertical transport of momentum (Fig. 7e, f). Thus, assuming the depth of the thermocline remains fixed in time, a *spring-neap switch* (rather than a cycle!) in mid-depth tidal shear (Figs. 2–3) can be attributed to variation in turbulence exchange. The associated factor-of-1.5 decrease in s has only weak counteracting effect. Surprisingly, this influence of the stratification on the vertical current structure is distributed equally on either side of the thermocline (Fig. 8).

The initially (day 140) parallel, in-phase (cf. Fig. 3b) and both anticyclonic current ellipses become wider (thinner) by the same amounts above (below) the thermocline when the near-bottom Ekman number increases (day 141). The ellipse inclination veers equally anticlockwise (clockwise) due to a simultaneous increase (decrease) of especially the phase of the anticyclonic relative to the cyclonic current component (Fig. 7e, f). In the nondimensionalized Ekman model, the observations in Figure 8 are artificially mimicked by requiring the vertical averages of the rotary current components to be fixed numbers, regardless of the parameterization (average amplitudes all equal to one and average phases all equal to zero in Fig. 7). In physical terms, referring to (3), this implies a fixed ratio

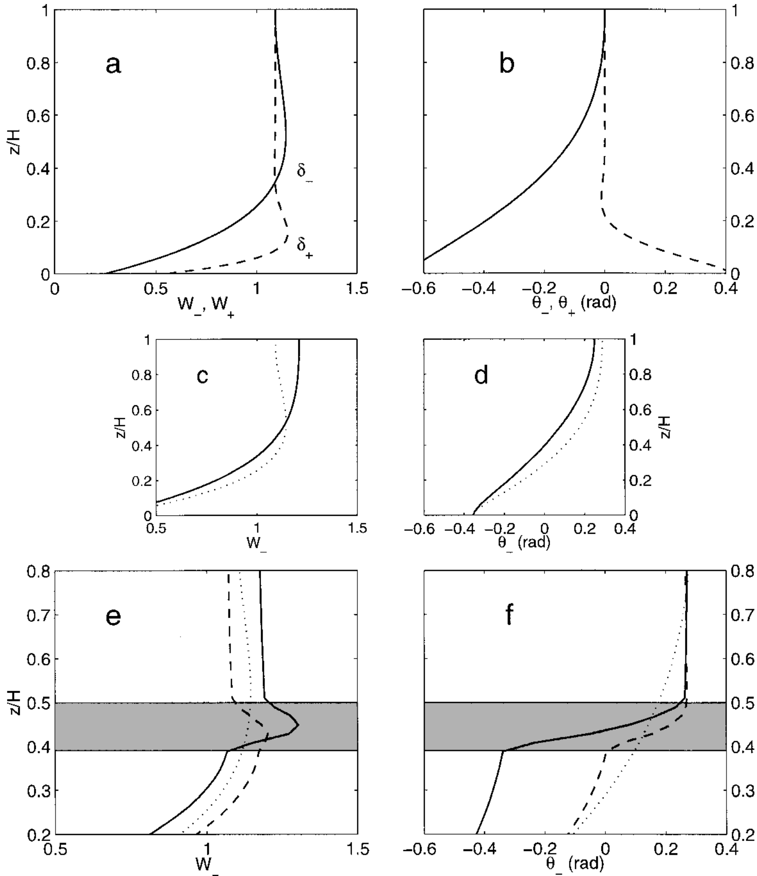

Figure 7. Examples of the vertical structure of currents oscillating at the tidal frequency, using a 1-D Ekman dynamics model. (a) Nondimensional amplitudes of rotary current components under well-mixed conditions for constant $E = 10^{-2}$ and $s = 10$ which fitted best observations made 10 miles off the INP site (Maas and van Haren, 1987). The location of the Ekman depths $\delta_{\pm}$ is arbitrary, their ratio not. (b) Phases corresponding to (a). (c) Anticyclonic rotary current amplitude under well-mixed conditions from (a) (dotted line) in comparison with one for $E = 2 \times 10^{-2}$ and $s = 7$, i.e. a doubling of the eddy viscosity (solid line). (d) Phases corresponding to (c). (e) Anticyclonic rotary current amplitude from (a) (dotted line) in comparison with the same component under stratified conditions. Mimicking stratification a three-layer model is used with $E_1 = E_3 = 10^{-2}$ in the surface and bottom boundary layers, $E_2 = 3 \times 10^{-4}$ in the thermocline (shaded) and $s = 10$ (dashed line; these parameters correspond to those used by Maas and van Haren, 1987). The solid line presents results for doubled eddy viscosities. Note restriction of the vertical range for clarity. (f) Phases corresponding to (e).

between the barotropic pressure gradient forcing and the internal frictional stresses, *besides* weakly turbulent coupling between surface and bottom well-mixed layers. Consequently, a decrease in turbulent coupling causes enhanced shear so that the weaker, cross-flow, current component becomes 180° out-of-phase across the thermocline, as observed.

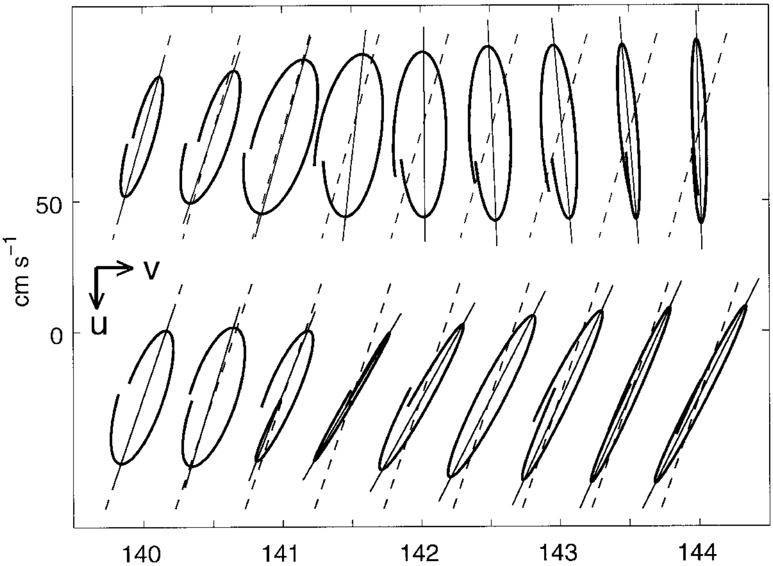

Figure 8. Band-pass filtered tidal and inertial data of the first half of Figure 3b, showing changes in tidally dominated current ellipses above (12 m depth, upper set of ellipses) and below the thermocline (23 m). The orientation of the ellipses is rotated by 90° for clarity, and the major axis of each ellipse (thin solid lines) is given relative to the first ellipses (dashed lines). All ellipses have an anticyclonic with time rotation sense. There is little vertical change in major-axis orientation initially. The sudden change in orientation above and below the thermocline at day 141.5 marks the onset of enhanced circularly polarized tidal shear. This shear amplitude remains constant as the ellipse orientations remain virtually the same toward springs (at day 145). The ellipses narrow due to an enhanced cyclonic relative to anticyclonic pressure gradient term in (3).

Shear can be enhanced by either increasing its amplitude or by increasing the angle between the current vectors above and below the thermocline. The latter is maximal when the vertical phase differences for the current components are 180°. While this is typical for linear mode-1 internal waves governed by inviscid ($A_2 = 0$) physics, it may also occur for barotropic oscillatory flows under viscous conditions varying with depth. Defining shear as 'optimal' when the maximum phase difference is found in at least one current component, its occurrence following a decrease in turbulent exchange is explained as follows for the extreme case of an initially rectilinear tidal current.

With a purely rectilinear near-surface u-current in the well-mixed (subscript m) case, so that $w_{+m}(z/H = 1) = w_{-m}(1)$, $\theta_{+m}(1) = \theta_{-m}(1) = 0$ we have an initial reference cross-flow amplitude at mid-depth of $V_m(0.5) = |w_{-m}(1) - w_{-m}(0.5)|$. When stratification (subscript s) appears, and assuming from (6) that $w_{+s}(z/H) = w_{+m}(z/H) = w_{-m}(1)$ for $z \gg \delta_+$, we are interested in the development of the cross-flow phase difference

$$\Delta\varphi_v = \tan^{-1}(Re(B), Im(B)), \quad \text{where} \quad B = \tilde{v}_s(z_1) - \tilde{v}_s(z_2) = i\{w_{-s}(z_1) - w_{-s}(z_2)\}, \quad (8)$$

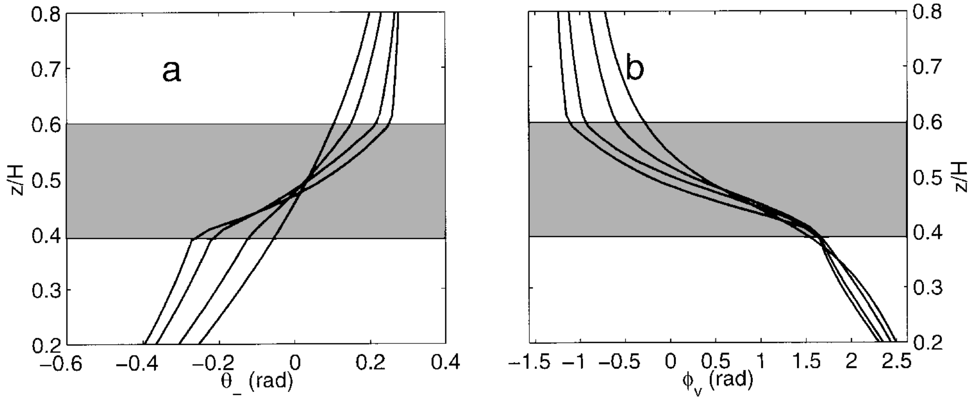

Figure 9. Effects of stratification on the vertical structure of cross-flow phase for a near-surface rectilinear tidal current as inferred from a three-layer Ekman model. Parameters are $s = 10$, $E_1 = E_3 = 2 \times 10^{-2}$ in surface and bottom boundary layers, and varying $E_2 = 2 \times 10^{-2}, 10^{-2}, 2 \times 10^{-3}, 4 \times 10^{-4}$ (about the value used in Fig. 7e, f) in the thermocline (shaded). The thermocline is twice as thick as in Figure 7 for clarity. This has (virtually) no consequences for the vertical phase changes. (a) Anticyclonic rotary current phases. The family of curves shows an increasing vertical phase difference for decreasing E_2. (b) North current phases, with similar dependency on E_2 as in (a).

as a function of E_2 for a thermocline between depths z_1 and z_2. This is mimicked using the Ekman model.

Varying $A_2 = (1.0 \rightarrow 0.02)A_1$ causes a variation in the vertical anticyclonic rotary component phase difference $\Delta\theta_- \approx 7° \rightarrow 30°$ so that $\Delta\varphi_v \approx 90° \rightarrow 180°$ (Fig. 9). Consequently, optimal cross-flow shear may be generated while viscosity still controls ($A_2 \neq 0$) vertical momentum transport under stratified conditions. This viscous control is also inferred from measurements (Figs. 3, 8) by comparing timing of maximal cross-flow shear with the moment of maximum current, as explained below.

As the motions are still nearly rectilinear, the u-current is also near its maximum when the current is maximal. Therefore, maximum v-shear is approximately in phase with the average u-current and, consequently, maximum u-shear occurs when the u-current is minimal (Fig. 10). As each shear component consists of vertical variations in amplitude and phase which are in quadrature with each other, e.g. $\partial u/\partial z = \partial U/\partial z \cos(\varphi_u - \sigma' t) - U\partial\varphi_u/\partial z \sin(\varphi_u - \sigma' t)$, implies that the shear observed here is dominated by vertical changes in phase because each current component is in quadrature with its associated shear component. This is in accordance with Ekman dynamics, following (8) and Figures 7, 9.

The relatively small change in amplitude across the stratification can be inferred directly from the ellipse rotation sense, which remains the same (Figs. 7e, 9, 10). Note that the ellipse rotation sense varies on modulation time scales, for example spring-neap as observed (Figs. 2, 9), when the current ellipses of the single harmonics (e.g., M_2, S_2) within a particular frequency band have any different inclinations. Such variation does not affect

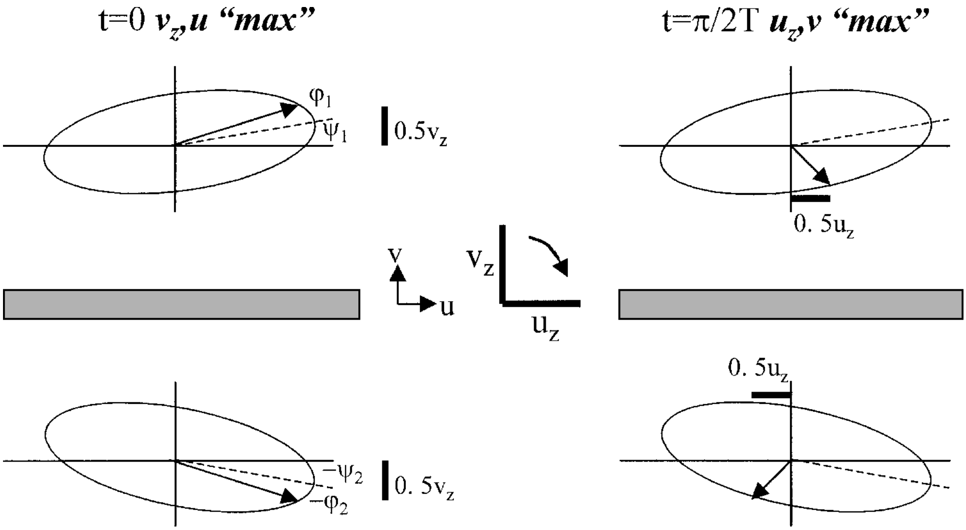

Figure 10. Impression of enhanced barotropic tidal current shear across stratification based on observations (Figs. 3, 5 and 8) and the Ekman model (Fig. 7). Enhanced shear is dominated by phase changes of the anticyclonic current components above and below (subscripts 1, 2) the thermocline with weak but non-zero viscosity. Initially, ellipse inclinations $\psi_1 = \psi_2 = 0$, the main axes being aligned with the *x*-axis. When stratification (shaded area) develops near mid-depth, the anticyclonic phases become enhanced ($\theta_{-1} > 0$)/decreased ($\theta_{-2} < 0$) above/below the stratification by equal amounts, so that, following (1), $\varphi_1 = \psi_1 > 0$, $\varphi_2 = \psi_2 = 360° - \varphi_1$. As the amplitudes are nearly unaffected by the stratification, the same (anticyclonic) rotation senses of the ellipses result in equal timing of the maxima of mean along-flow current, in the direction of the semi-major axis, and cross-flow shear (left panel). Maximum mean cross-flow current and along-flow shear follow a quarter period later (right panel). Both shear components are equal in magnitude and the rotation sense of the shear vector is anticyclonic (central panel). The partial derivative $\partial/\partial z$ is denoted by the subscript z.

above observations, because Ekman dynamics do not vary much within a limited (e.g. semidiurnal tidal) frequency band, as long as the ellipse rotation senses are indeed the same above and below the thermocline. The observed timing of maximum shear and current components is unlikely attributable to freely propagating mode-1 internal tidal waves (with ellipticity controlled by σ/f), as it restricts baroclinic tidal currents to exactly $\pm 90°$ phase difference with the main barotropic flow.

Near the Dutch coast, the vertical tidal current structure across stratification is also not dominated by mode-1 internal waves. Nonetheless, viscosity control is less important (Visser *et al.,* 1994). The relative ellipse inclination flips from clockwise to anticlockwise veering toward the bottom, the ellipse rotation sense changes from anticyclonic to cyclonic across the stratification, and the maximal cross-shore shear appears when the current is minimal. This cannot be explained following the above Ekman arguments, as this requires that the mid-depth shear be dominated by vertical changes in amplitude rather than phase, with no possible explanation for observed vertical variation of 180° in the phase of one of the current components. Alternatively, Visser *et al.* (1994) attribute the first-mode appearance of cross-shore flow to the coastal boundary condition of zero cross-shore transport.

Although the coast does not affect the observed variation in the tidal current ellipses with depth in the central North Sea, it influences generation of inertial motions. As $\sigma \to f$, rotation of the frame of reference for the anticyclonic component approaches zero, and the corresponding Ekman number becomes infinite. From their observations, Maas and van Haren (1987) concluded that mode-1 inertial currents are embedded in a fluid with nonzero low-frequency relative vorticity. Then, an effective inertial frequency (Mooers, 1975; Kunze, 1985) $f_0 = f + 0.5(\partial v_0/\partial x - \partial u_0/\partial y)$ should replace f, so that the apparent Ekman number $E^0_{-f} = E \cdot f/|f_0 - f|$ remains finite.

In a fluid containing weak low-frequency relative vorticity, generated by horizontal current differences of $O(1 \text{ cm s}^{-1} \text{ km}^{-1})$ or less, E^0_{-f} is larger than the 'tidal Ekman number.' Then, with reference to Figure 7e, f for the effects of increased Ekman numbers in the well mixed layers above and below a thermocline on shear across it, near-inertial motions are more affected by stratification than the anticyclonic component of the tidal current. This justifies a slab-layer model for the generation of inertial motions by wind-stress as has been employed successfully by Pollard and Millard (1970) and Krauss (1979), who implicitly modeled a viscous and an inviscid layer above and inside the thermocline, respectively.

Such surface slab-layer inertial motion generates a first-mode response within a typical timescale of $2/f$ through the coastal boundary condition (Krauss, 1979; Millot and Crépon, 1981). Consequently, in a two-layer rather than continuously stratified water column, inertial shear automatically exhibits a 180° phase difference between *both* current components above and below a thermocline. As inferred from observations by Krauss (1981), inertial shear across the near-surface thermocline is dominated by a change in phase (Fig. 11), where the anticyclonic inertial shear is split according to (7). However, in shallow seas like the North Sea viscosity cannot be completely neglected due to the proximity of the bottom, and due to internal turbulence generation.

Under purely inviscid physics, the amplitude of the hypothetical mode-1 vertical current structure is constant with depth, except for a singularity at the 180° phase change, within the thermocline. When this mode-1 structure becomes frictionally modified, being still in an environment of nonzero low-frequency vorticity, it will smooth its phase change symmetrically across a layer of finite depth, while at its center the amplitude becomes minimal, albeit not necessarily zero (Fig. 15 in Maas and van Haren, 1987). *In contrast,* a vertical current structure uniquely governed by Ekman dynamics may even show an amplitude *maximum* at the thermocline, with both amplitude and phase changes *asymmetrically* distributed across a layer of constant reduced viscosity (Fig. 7). Both types of shear can be inferred from average (Fig. 11) and individual (Fig. 12) vertical profiles of shear or currents, respectively.

Knowing that inertial motions are maximal near the surface, one observes an amplitude

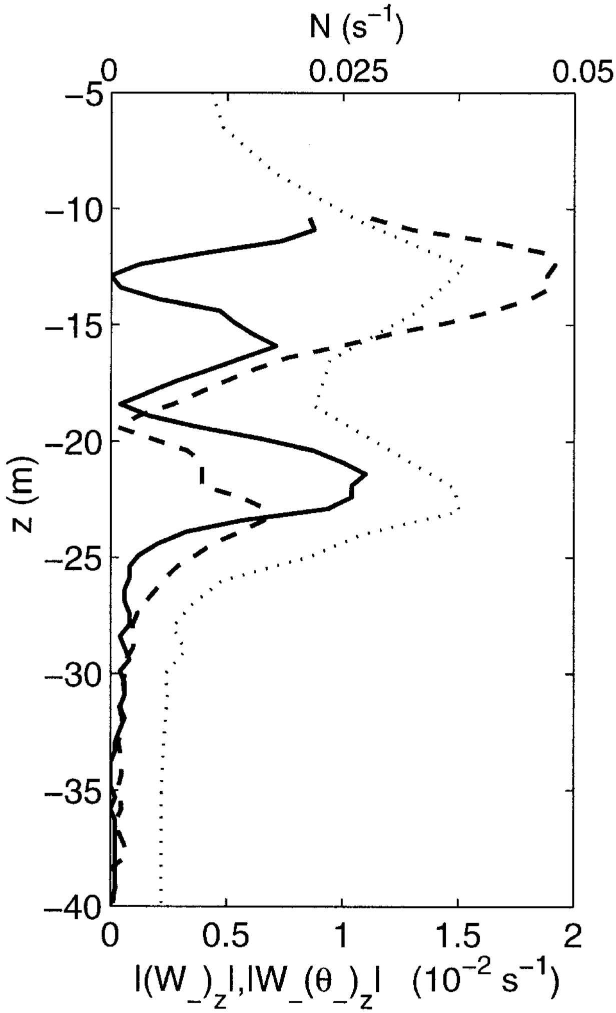

Figure 11. Rms buoyancy frequency N (dotted line; scale on top) compared with the absolute values of the amplitude ($|W_{-z}|$, solid line; subscript z denoting a partial derivative) and phase parts ($|W_{-}\theta_{-z}|$, dashed line) of anticyclonic rotary shear component harmonically analysed at the inertial frequency for the period between days 194–202.

minimum at the upper thermocline (Fig. 11 and Fig. 12a) where the phase change dominating the shear is symmetrically distributed (Fig. 11). The observed phase change dominating mode-1 shear is understood because $\Sigma|W_{-z}| < 2|W_{-}| < \pi|W_{-}| \approx \Sigma|W_{-}\theta_{-z}|$, summed across the stratification. Across the lower thermocline, the shear components are distributed asymmetrical with a change of phase dominating closest to the bottom mixed layer (Fig. 11). In order to smoothly transfer momentum vertically across varying viscosity, the largest shear is found on that side of the thermocline closest to its source, according to

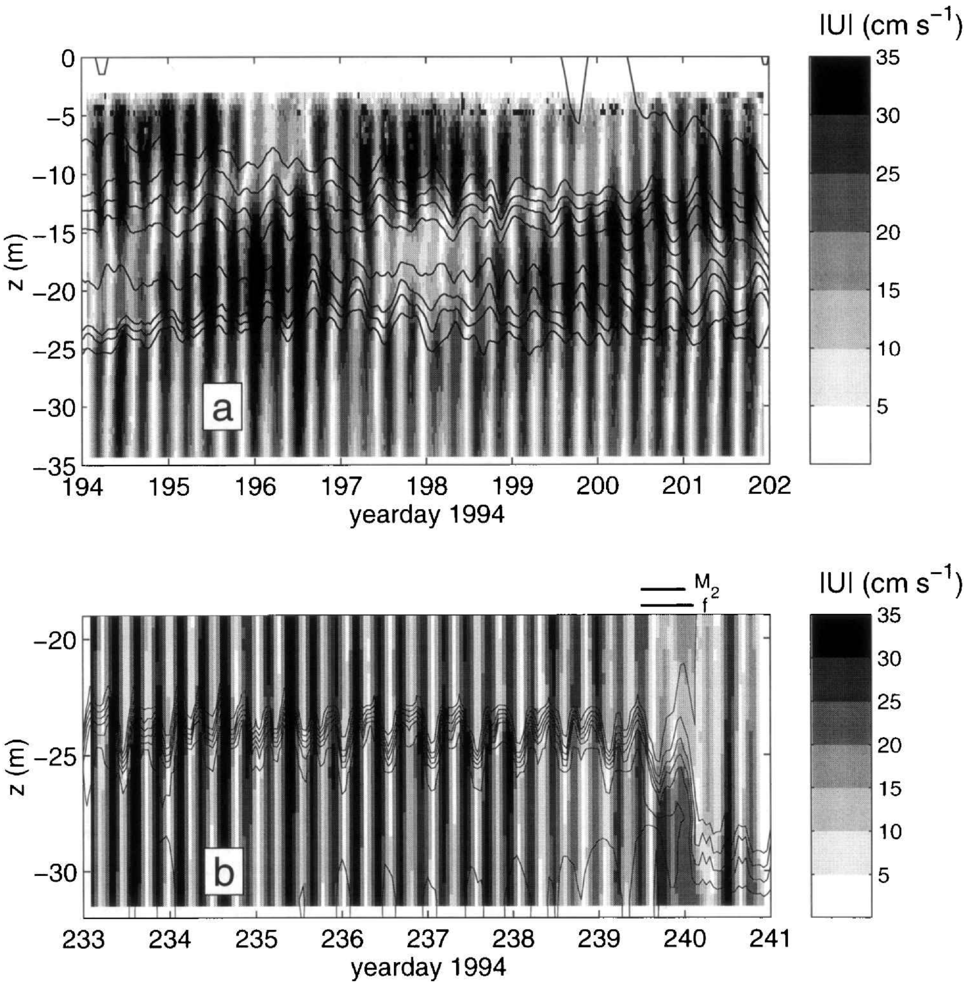

Figure 12. Total current amplitudes for the periods in Figure 1. (a) Mid-summer period. Below 25 m depth the motions are basically semi-diurnal tidal, influenced by bottom friction. They show a smooth transition in amplitude across the lower thermocline. Above the latter, inertial and semi-diurnal tidal motions are roughly equal in size (note the $M_2 - f$ beat), with inertial shear dominating across the upper part of the lower thermocline and across the upper thermocline. This is mode-1 baroclinic shear, with amplitude minima at the thermocline (best visible e.g. at $z = -13$ m around days 195, 197 and 199). (b) Late-summer period, with dominating frictionally modified barotropic semi-diurnal tidal shear. In contrast with (a) no amplitude minimum is found at the thermocline.

Ekman dynamics (Figs. 7, 9). The strong amplitude shear across the lower thermocline in Figure 11 is typical for inertial motions only, as the apparent Ekman number is large in the bottom mixed layer. Semidiurnal tidal shear is not dominated by a change in amplitude across the same thermocline (Fig. 12).

This particular sensitivity of shear to vertical changes in phase of the current allows distinguishing the dominant frequency of the shear and separation of barotropic from mode-1 motions within the thermocline itself. This requires observations that resolve the typical thermocline thickness (Figs. 11–13), which may become small in shallow seas (<2 m), but never infinitesimally thin. This is attributable to stability (Richardson number) control, which is discussed below.

6. Discussion

The suggested explanation for the observed relationship between stratification and vertical current shear, partially in terms of Ekman dynamics, needs validation of its implications for vertical mixing. This requires a proper model for the stabilizing mechanism following (growing) instability, or for limitation to growth of destabilizing shear by stratification. For shelf seas, one needs the exact location of the stratification and the characteristic mid-depth shear generation mechanism, as well as knowledge of the turbulence-generating mechanisms at the external boundaries. Ideally, because enhanced stratification itself does not invoke vertical turbulent exchange, the precise mechanism leading to diapycnal mixing has to be captured. Breaking internal waves have been suggested (Linden, 1979; Gregg and Kunze, 1991; Polzin, 1996).

Existing models do not include the breaking of internal waves or even a proper parameterization. Naturally, such vertical exchange is not reproduced by simple Ekman dynamics, in which the depth, thickness and strength of the enhanced stratification are prescribed. What can be learned from this model and the North Sea observations is the importance of incorporation of vertical exchange across stratification in future modeling. This exchange is likely due to internal shear-driven turbulence. The most predictable (barotropic!) tidal shear requires the modeling of spatial (Prandle, 1982; Soulsby, 1983) and, surprisingly, weakly temporal (Figs. 2–3) variations in the relative contributions to the shear from the rotary components. Superposed on the tidal shear is the potentially more important inertial shear. Unfortunately, inertial motions, and even more so inertial shear, are less predictable than tidal currents. The data presented here may shed some light on the relative importance of inertial shear across stratification.

Like tidal shear, mid-depth inertial shear is weak in a well-mixed water column. It is predominantly initiated by suitable atmospheric forcing during neaps, or when stratification extends high into the water column, usually under calm weather conditions. In both cases, tidal shear across stratification is relatively weak. Indirectly, this (re)confirms the importance of slab-layer generation of inertial motions, provided weak tidal shear across stratification is interpreted as a reduction of overall viscosity so that enhanced destabilization is only governed by the developing inertial shear.

For both tidal and inertial shear dominance, the shear magnitude is 'constant' with time. At least one current component is 180° out-of-phase across the thermocline, so that the shear and the possible relationship between shear and stratification (through Ri) are controlled by variations in the amplitude of this optimal shear component. Following observations, also stratification is 'constant' with time. Then, $Ri \approx$ constant and sufficient turbulent dissipation occurs to maintain Ri at a marginally stable state.

Using the results from the Ekman model, constant shear magnitude implies a 'constant' momentum transfer coefficient ($A \propto |\mathbf{S}|^{-1}$), as implicitly modeled using continuity of current velocity and shear stress at the upper and lower limits of the thermocline. Adopting earlier results from microstructure observations that $K \propto N^{-1}$ (Gargett, 1984; Moum and Osborn, 1986), gives an eddy Prandtl number ($Pr = A/K$) constant with time when the flow is marginally stable. A likely value is $Pr \approx 1$, as average values of $A \approx K = 5 \times 10^{-5}$ m^2 s^{-1} are estimated across the thermocline from the fitting of observations with the Ekman model and from consideration of near-bottom temperature variations due to diffusion, respectively.

These results are different from the open ocean. The quoted K-scaling is disputed for a canonical open ocean internal wave field, where more likely $K \propto$ constant (e.g. Polzin *et al.,* 1995). These authors indicate that a different, unspecified K-scaling may be valid for a noncanonical internal wave field, such as found above sloping bottoms. There, internal wave breaking following (critical) reflection is expected to dominate vertical exchange and $Pr \approx 100$ was observed by van Haren *et al.* (1994). Perhaps the value of $Pr \approx 1$ found here represents noninternal wave shear across stratification affecting breaking rather than generation of high-frequency internal waves producing (sporadic) turbulence. Recent results from direct flux measurements above sloping and flat bottoms confirm these Pr-values (J. R. Gemmrich, pers. comm., 2000).

This $Pr \approx 1$ points to a near-critical value of Ri as it points at a dominance of a fully turbulent exchange over momentum absorption by internal waves with the flux Richardson number, expressing the ratio of the removal of turbulent energy by buoyancy forces and its production by shear, roughly equaling Ri (Turner, 1979).

A critical transition value of $Ri = 0.25$ is reported following linear stability theory by Miles (1961) and Howard (1961), while a transition value of $Ri \approx 1$ is suggested for a breakdown of nonlinear flow (Abarbanel *et al.,* 1984). At the depths of enhanced stratification, observed $0.25 < Ri < 1$ (see also van Haren *et al.,* 1999), similar to internal-wave-induced shear instability values reported for shallow estuaries (Uittenbogaard, 1995) and the open ocean (Polzin, 1996). Further studies are recommended on the nonlinearity of flow in stratified natural waters. In the North Sea, possibly important are nonlinear interactions inside the internal wave band, as may be inferred from Figure 13, where the appearance of enhanced (yet much weaker than tidal or inertial) shear at interaction frequencies M_4 and $M_2 + f$ may stimulate such study.

7. Conclusions

In this paper, detailed current and temperature observations from the seasonally stratified central North Sea are presented to study the relationship between vertical current shear and stratification. Semidiurnal tidal and inertial currents dominate. Under stratified conditions and in contrast with inertial currents, the vertical tidal current structure and

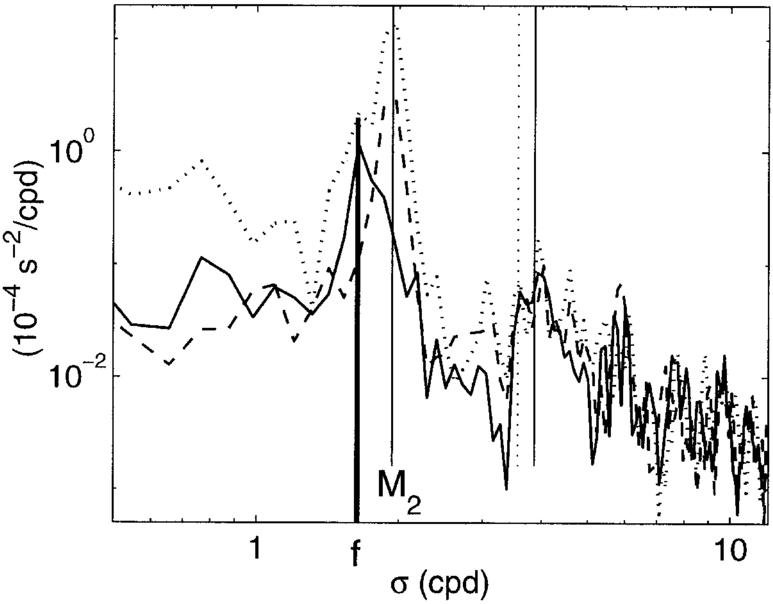

Figure 13. Shear spectra from days 230–240, using 3 degrees of freedom, for different depths and vertical scaling. The dotted line represents the spectrum of current difference between 19–28 m depth scaled by 2 m (constant thermocline thickness). Solid and dashed lines represent ADCP observations of shear within the thermocline at the lowest possible vertical resolution of 0.5 m at on average 23.2 m and 24.8 m depth, respectively. The ADCP shear spectra are computed in isotherm-following coordinates for clarity, but the essentials are no different in the Eulerian frame of reference. The thick vertical line denotes the inertial frequency, the thin solid lines M_2 and M_4, and the dotted line $M_2 + f$.

shear are not predominantly governed by inviscid physics, confirming earlier reports (Maas and van Haren, 1987; van Haren and Maas, 1987; Howarth, 1998). It is found that,

- the largest shear is confined to the depth of largest stratification. Its magnitude varies with time following the spring-neap cycle and changes with wind-stress magnitude.
- Inertial shear dominates after strong winds *as well as* during calm weather if stratification is not concentrated in a thin layer, while semidiurnal tidal shear dominates otherwise, particularly during springs.
- At both frequencies, the shear components have equal amplitudes, the vector rotating anticyclonically with time along a circular path, such that shear magnitude is 'constant' with time, even though tidal currents are nearly rectilinear.
- The tidal shear's anticyclonic rotation with time can be explained by Ekman dynamics with a turbulent viscosity which varies over longer timescales than tidal periods.
- In a shallow sea where Ekman depths are comparable with the water depth, tidal shear

determines the vertical extent of the well-mixed bottom boundary layer through turbulence shear production. Therefore, it influences the location of the thermocline, and becomes modified in turn by the change in eddy viscosity at the depth of the thermocline. Ekman dynamics favor shear across stratification for frequencies closest, but not equal, to the local inertial frequency, for which the (anticyclonic) Ekman depth is largest. Thus, the rotating water column acts like a filter in frequency for the shear.

- Monitoring the timing of shear and current components across stratification allows distinction between currents controlled by (reduced) viscosity, with maximum cross-flow shear occurring when the current is near maximal (Fig. 10), and by inviscid physics. Viscosity control implies shear dominated by a vertical change in phase of the currents with little change in amplitude. Inviscid flow requires an amplitude minimum inside the thermocline.
- Lateral boundary conditions are more important for near-inertial motions. Anticyclonic with time inertial shear develops because the stratified layer below a near-surface well-mixed layer is interpreted as inviscid. Viscosity smooths this inertial shear across finite depths.
- As near-inertial motions are generated near the surface and tidal momentum transfer is imposed through bottom friction, the dominant frequencies of the shear components can be distinguished within a thermocline itself. The thermocline acts like a filter in the vertical for the shear.
- Enhanced inertial shear reduces the gradient Richardson number to near-critical values within a thermocline. A thermocline never becomes infinitesimally thin, because of Ri control just above the critical value. Such marginal stability is accompanied by an (indirectly inferred) eddy Prandtl number of about 1, implying turbulent transfer across the thermocline in equilibrium with the shear, the latter possibly causing breaking rather than generation of high-frequency internal waves.

Some support for such turbulent diapycnal exchange, not being generated at the surface and bottom boundaries but internally following a subtle balance between shear and stratification, is obtained from laboratory and estuary observations. As most shelf seas are dominated by barotropic tidal motions, the tidal shear analyses presented here are likely valid for other shallow seas' areas outside the North Sea, provided they are not too close to the coast (say, more than half an external Rossby radius away). The depth should be comparable to the (anticylonic) Ekman depth. When the depth is larger, inertial shear becomes unaffected by tidal shear. Although the North Sea is a complex, and often rough, natural environment, it may be ideal for further studies on detailed mechanisms of diapycnal exchange, viz. of the effects of nonlinearity on oceanic flows, in relation with the marginal stability across stratification rendered by tidal and inertial shear.

Acknowledgments. For his continuous support and a critical review of this paper, I would like to express my gratitude to Leo Maas. This paper benefitted from comments by two anonymous referees. I thank the crew of the R. V. *Pelagia* for their pleasant cooperation. During INP (Integrated North Sea Programme), I have been supported by a grant from the Netherlands Organization for the Advancement of Scientific Research, NWO. This is NIOZ publication 3342.

REFERENCES

Abarbanel, H. D. I., D. D. Holm, J. E. Marsden and T. Ratiu. 1984. Richardson number criterion for the nonlinear stability of three-dimensional stratified flow. Phys. Rev. Lett., *52,* 2352–2355.

Eckart, C. 1948. An analysis of the stirring and mixing processes in incompressible fluids. J. Mar. Res., *7,* 265–275.

Gargett, A. E. 1984. Vertical eddy diffusivity in the ocean interior. J. Mar. Res., *42,* 359–393.

Gill, A. E. 1982. Atmosphere-Ocean Dynamics, Academic Press Inc., Orlando, 662 pp.

Gonella, J. 1972. A rotary-component method for analyzing meteorological and oceanographic vector time series. Deep-Sea Res., *19,* 833–846.

Gregg, M. C. and E. Kunze. 1991. Shear and strain in Santa Monica Basin. J. Geophys. Res., *96,* 16709–16719.

Howard, L. N. 1961. Note on a paper of John W. Miles. J. Fluid Mech., *10,* 509–512.

Howarth, M. J. 1998. The effect of stratification on tidal current profiles. Cont. Shelf Res., *18,* 1235–1254.

Krauss, W. 1979. Inertial waves in an infinite channel of rectangular cross section. D. Hyd. Z., *32,* 248–266.

—— 1981. The erosion of the thermocline. J. Phys. Oceanogr., *11,* 415–433.

Kunze, E. 1985. Near-inertial wave propagation in geostrophic shear. J. Phys. Oceanogr., *15,* 544–565.

Lamb, Sir H. 1975. Hydrodynamics, Cambridge University Press, Cambridge, 738 pp.

Linden, P. F. 1979. Mixing in stratified fluids. Geophys. Astrophys. Fluid Dyn., *13,* 3–23.

Maas, L. R. M. and J. J. M. van Haren. 1987. Observations on the vertical structure of tidal and inertial currents in the central North Sea. J. Mar. Res., *45,* 293–318.

Miles, J. W. 1961. On the stability of heterogeneous shear flows. J. Fluid Mech., *10,* 496–508.

Millot, C. and M. Crépon. 1981. Inertial oscillations on the continental shelf of the Gulf of Lions-Observations and theory. J. Phys. Oceanogr., *11,* 639–657.

Mooers, C. N. K. 1975. Several effects of a baroclinic current on the cross-stream propagation of inertial-internal waves. Geophys. Fluid Dyn., *6,* 245–275.

Moum, J. N. and T. R. Osborn. 1986. Mixing in the main thermocline. J. Phys. Oceanogr., *16,* 1250–1259.

Munk, W. H. and E. R. Anderson. 1948. Notes on a theory of the thermocline. J. Mar. Res., *7,* 276–295.

Pollard, R. T. and R. C. Millard Jr. 1970. Comparison between observed and simulated wind-generated inertial oscillations. Deep-Sea Res., *17,* 813–821.

Polzin, K. 1996. Statistics of the Richardson number: mixing models and finestructure. J. Phys. Oceanogr., *26,* 1409–1425.

Polzin, K., J. M. Toole and R. W. Schmitt. 1995. Finescale parametrization of turbulent dissipation. J. Phys. Oceanogr., *25,* 306–328.

Prandle, D. 1982. The vertical structure of tidal currents. Geophys. Astrophys. Fluid Dyn., *22,* 29–49.

Sherwin, T. J. 1988. Measurements of current speed using an Aanderaa RCM4 current meter in the presence of surface waves. Cont. Shelf Res., *8,* 131–144.

Soulsby, R. L. 1983. The bottom boundary layer of shelf seas, *in* Physical Oceanography of Coastal and Shelf Seas, B. Johns, ed., Elsevier, Amsterdam, 189–266.

—— 1990. Tidal-current boundary layers, *in* The Sea, B. Le Mehaute and D. M. Hanes, eds., Wiley-Interscience, NY, 523–566.

Turner, J. S. 1979. Buoyancy Effects in Fluids, Cambridge University Press, Cambridge, 368 pp.

Uittenbogaard, R. E. 1995. The importance of internal waves for mixing in a stratified estuarine tidal flow. PhD-thesis, Delft University, 320 pp.

van Haren, J. J. M. and L. R. M. Maas. 1987. Temperature and current fluctuations due to tidal advection of a front. Neth. J. Sea Res., *21,* 79–94.

van Haren, H., L. Maas, J. T. F. Zimmerman, H. Ridderinkhof and H. Malschaert. 1999. Strong inertial currents and marginal internal wave stability in the central North Sea. Geophys. Res. Lett., *26,* 2993–2996.

van Haren, H., N. Oakey and C. Garrett. 1994. Measurements of internal wave band eddy fluxes above a sloping bottom. J. Mar. Res., *52,* 909–946.

Visser, A. W., A. J. Souza, K. Hessner, and J. H. Simpson. 1994. The effect of stratification on tidal current profiles in a region of freshwater influence. Oc. Acta, *17,* 369–381.

Received: *2 February 1999;* revised: *28 February, 2000.*